

Cracked Continuum Modeling of Reinforced Concrete Elements under Impact

Serhan Guner, Trevor D. Hrynyk, and Andac Lulec

Synopsis: Current computational modeling approaches used to evaluate the impact-resisting performance of reinforced concrete infrastructure generally consist of high-fidelity modeling techniques which are expensive in terms of both model preparation and computation cost; thus, their application to real-world structural engineering problems remains limited. Further, modeling shear, erosion, and perforation effects presents as a significant challenge, even when using expensive high-fidelity computational techniques. To address these challenges, a simplified nonlinear modeling methodology has been developed. This paper focuses on this simplified methodology which employs a smeared-crack continuum material model based on the constitutive formulations of the Disturbed Stress Field Model. The smeared-crack model has the benefit of simplifying the modeling process and reducing the computational cost. The total-load, secant-stiffness formulation provides well-converging and numerically stable solutions even in the heavily damaged stages of the responses. The methodology uses an explicit time-step integration method and incorporates the effects of high strain rates in the behavioral modeling of the constituent materials. Structural damping is primarily incorporated by way of nonlinear concrete and reinforcement hysteresis models and significant second-order mechanisms are considered. The objective of this paper is to present a consistent reinforced concrete modeling methodology within the context of four structural modeling procedures employing different element types (e.g., 2D frames, 3D thick-shells, 3D solids, and 2D axisymmetric elements). The theoretical approach common to all procedures and unique aspects and capabilities of each procedure are discussed. The application and verification of each procedure for modeling different types of large-scale specimens, subjected to multiple impacts with contact velocities ranging from 8 m/s (26.2 ft/s) to 144 m/s (472 ft/s), and impacting masses ranging from 35 kg (77.2 lb) to 600 kg (1323 lb), are presented to examine their accuracy, reliability, and practicality.

Keywords: axisymmetric, erosion, frame, missile, perforation, shear, shell, smeared, solid, strain rates.

ACI member **Serhan Guner** is an Assistant Professor in the Department of Civil and Environmental Engineering at the University of Toledo, OH, USA. He received his PhD from the University of Toronto, Toronto, ON, Canada. He is a member of the Joint ACI-ASCE Committee 447-Finite Element Analysis of Reinforced Concrete Structures, 370-Blast and Impact Load Effects, and 123-Research and Current Developments. His research interests include finite element modeling of concrete structures and foundations, shear effects in concrete, deep beams and disturbed regions, structural response to extreme loads, and development of numerical modeling methods and associated software.

ACI member **Trevor D. Hrynyk** is an Assistant Professor in the Department of Civil and Environmental Engineering at the University of Waterloo, Waterloo, ON, Canada. He received his PhD from the University of Toronto, Toronto, ON, Canada, in 2013. He is a member of the Joint ACI-ASCE Committees 447-Finite Element Analysis of Reinforced Concrete Structures, 421-Design of Reinforced Concrete Slabs, and 445C-Shear & Torsion. His research interests include analysis of reinforced concrete structures, response under extreme loads, and damage assessment.

Andac Lulec is an Engineer in Training at BBA E&C Inc., Toronto, ON, Canada. He received his PhD from the University of Toronto, Toronto, ON, Canada, in 2017. His research interests include analysis of reinforced concrete structures under impact and blast loads.

INTRODUCTION

Structural resilience to impact loads has become an important design requirement for strategic buildings due to increased security concerns. Modeling techniques used for extreme load scenarios, such as impact, range from simplified single-degree-of-freedom (SDOF) methods to sophisticated high-fidelity finite element analysis (FEA) procedures. While SDOF methods are highly practical and directly provide the required design parameters, they are best suited for the analysis of individual structural elements and do not account for important influences such as the interaction of shear force, axial force and bending moment responses, membrane action, and hysteretic material response (see El-Dakhkhni 2010). High-fidelity FEA techniques are more comprehensive but demand extensive modeling experience and special input parameters and thus take significant time. Further, the accuracy of the results obtained from the FEA techniques is often highly dependent on the input material and analysis parameters supplied by the user. In the case of modeling reinforced concrete (RC), a series of calibration studies involving the use of previously tested benchmark specimens are often required, arguably decreasing their practical applicability and increasing their cost. Thus, there remains a significant need for simplified, yet adequately accurate, analysis methods that can be used by structural engineers for the performance-based design and assessment of structures under extreme loading scenarios such as impact.

In response to this need, a simplified nonlinear modeling methodology, employing different types of finite elements, has been developed using experimentally verified material behavior models specifically developed for RC. The methodology employs a smeared-crack continuum material modeling approach based on the constitutive formulations of the Disturbed Stress Field Model (Vecchio 2000). The smeared-crack modeling approach simplifies the modeling process and aids in reducing computational cost. A total-load secant-stiffness formulation, along with a strain-based solution algorithm, is employed and shown capable of capturing heavily damaged stages of the impact response. The total-load secant-stiffness formulation also provides advantages by providing well-converging and numerically stable solutions, thereby further reducing computational costs. The primary objective of this paper is to present and assess the adequacy of this simplified nonlinear material modeling methodology applied in the context of four different structural modeling procedures (i.e., 2D frames, 3D thick-shells, 3D solids, and 2D/3D axisymmetric elements).

RESEARCH SIGNIFICANCE

Robust and cost-effective design for impact resilience requires advanced nonlinear modeling techniques to simulate the system-level behavior of concrete structures both in the pre- and post-peak stages of the response. This study describes a comprehensive modeling methodology specific to RC with the aim of simplifying the modeling process while still providing adequate response simulations even in the heavily damaged post-impact stages of the impact response.

MATERIAL MODELING AND ANALYSIS PARAMETERS

The following provides an overview of the RC material modeling approach and analysis parameters that are specifically relevant to the impact analysis of structural concrete infrastructure and are essentially common amongst the different structural modeling procedures presented in this paper (i.e., models developed by way of 2D frame elements, 3D thick-shell finite elements, 3D solid finite elements, and 2D axisymmetric finite elements).

Material Constitutive Models

Concrete behavioral modeling is performed in accordance with the formulations of the Disturbed Stress Field Model (DSFM) (Vecchio 2000), a cracked concrete dedicated material model developed as an extension to the Modified Compression Field Theory (MCFT) (Vecchio and Collins 1986). This smeared, hybrid rotating-fixed crack analysis procedure inherently considers the redistribution of internal forces that can occur due to local changes in stiffness arising from cracking or crushing of concrete, yielding of the steel reinforcement, concrete compression softening attributed to the presence of lateral tension, the presence of post-cracking concrete tensile stresses between crack locations, and the influences associated with variable and changing crack widths (including slip deformations along crack surfaces). Additional details regarding the implementation of the DSFM (which was originally developed to model the response of RC elements under biaxial stress conditions) in the context of the modeling procedures presented in this paper are provided elsewhere (e.g., Hrynyk and Vecchio 2015).

While cracked RC material modeling is principally done in accordance with the formulations of the DSFM, a library of advanced material behavior models for concrete, reinforcement, and their bond and interaction is available amongst the modeling procedures presented in this paper. To simplify the modeling process and permit cost-effective solutions for a given problem, one default model is recommended for each material behavior for applications commonly encountered in practice. These default material models are presented in Table 1.

Table 1 – Default material models (refer to Wong et al. 2013 for model formulations)

Material Behavior	Default Model	Material Behavior	Default Model
Compression base curve	Hognestad, Popovics or Hoshikuma et al.	Concrete hysteresis	Nonlinear w/ plastic offsets
Compression post-peak	Modified Park-Kent	Slip distortion	Walraven
Compression softening	Vecchio 1992-A	Strain rate effects	fib Model Code - Malvar
Tension stiffening	Modified Bentz 2003	Rebar hysteresis	Seckin w/ Bauschinger
Tension softening	Linear	Rebar dowel action	Tassios (Crack slip)
Confinement strength	Kupfer / Richart	Rebar buckling	RDM Model (Akkaya et al.)
Cracking criterion	Mohr-Coulomb (Stress)	Geometric nonlinearity	Considered
Crack width check	Agg/5 Max crack width	Previous loading history	Considered

The concrete hysteretic response (Fig. 1) associated with a RC element under load cycling is calculated using a plastic-offset modeling approach (Vecchio 1999) following a nonlinear Ramberg-Osgood formulation. Popovics (1973) and Modified Park-Kent (Mander et al. 1988, Scott et al. 1982, Kent and Park 1971) models are adopted to establish the backbone curves for the pre- and post-peak regions. Confinement effects are an inherent part of this response and modeled using the formulations of Kupfer et al. (1969) and Richart et al. (1928).

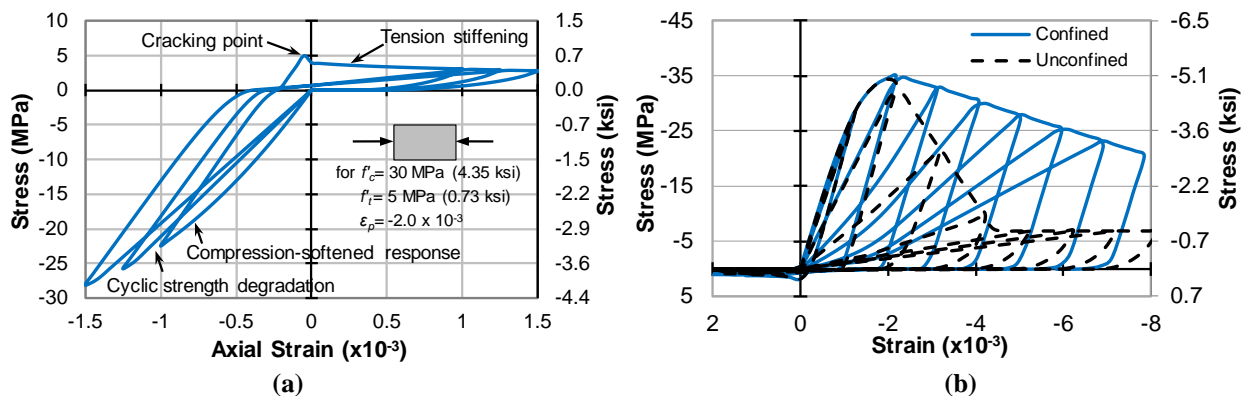


Fig. 1 – Concrete hysteresis model: (a) compression softening and tension stiffening effects; (b) confinement effects

The reinforcing steel hysteresis response is based on the Seckin model with Bauschinger effect (Seckin 1981) in tension, and the RDM model (Akkaya et al. 2019) in compression as shown in Fig. 2. The RDM model accounts for the interactions between lateral ties and longitudinal bars and simulates the compressive stress-strain response of reinforcing bars, including the onset of inelastic buckling and subsequent degradation in the post-buckling regime. Formulation details and the open-access code of the RDM model can be obtained from Akkaya et al. (2019).

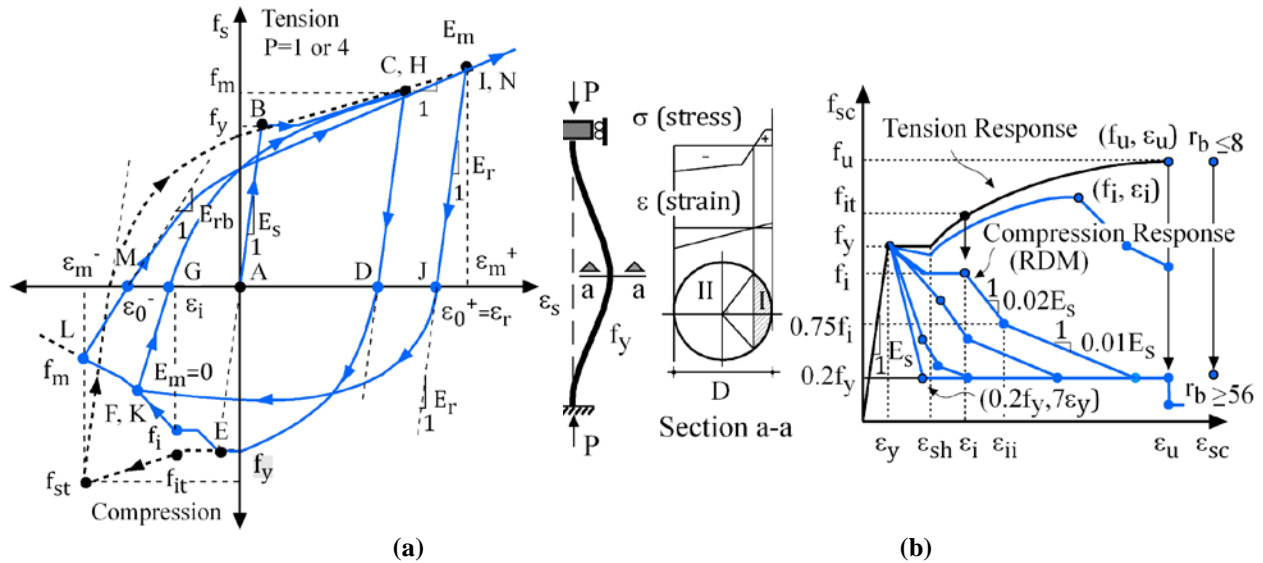


Fig. 2 – Reinforcing bar hysteresis model: (a) including Bauschinger and buckling effects; (b) backbone curves for buckling parameter r_b ranging from 8 to 56 (Akkaya et al. 2019)

Solution Algorithm

Relevant to the impact analyses, an explicit three-parameter time-step integration method is employed for the solution of the dynamic equation of motion. Unlike most other procedures, a total-load secant-stiffness formulation is derived to improve the convergence and provide compatibility with the constitutive models employed. The formulations are based on three parameters, γ , β , θ , which allows the use of either Newmark's Average Acceleration, Newmark's Linear Acceleration (Newmark 1959), or Wilson's Theta (Wilson et al. 1973) methods. An overview of the formulation details can be found in Guner and Vecchio (2010, 2012).

Strain Rates

When subjected to high rates of loading, concrete and reinforcing steel materials exhibit increased strength. This strength gain is considered through a dynamic increase factor (DIF) approach, in which the strain rate values for each concrete and steel layer are determined from the slope of the strain-time response. The corresponding DIFs are calculated and applied to the static material properties. Numerous studies have experimentally investigated the relationship between the strain rates and the material properties. The experimental data shown in Fig. 3 confirms the general trend with differing response curves. In this study, the *fib* Model Code (2010) formulations are employed for concrete because they represent the lower bound values. The Malvar (1998) formulations are selected as default for the reinforcing steel to provide conservative response simulations for concrete- or shear-dominated cases common in members subjected to impact loads. The lower bound CEB (1988) formulations can also be used when appropriate.

Structural Damping

The actual damping associated with the computed impact responses are primarily accounted for by the steel reinforcement and cracked concrete material hysteresis models. In addition, supplementary damping can be defined to enhance the solution stability as needed, or improve the damping response for low damage or primarily linear elastic response cases. The details regarding the supplementary damping levels, if any, are presented in the following sections on a case-by-case basis.

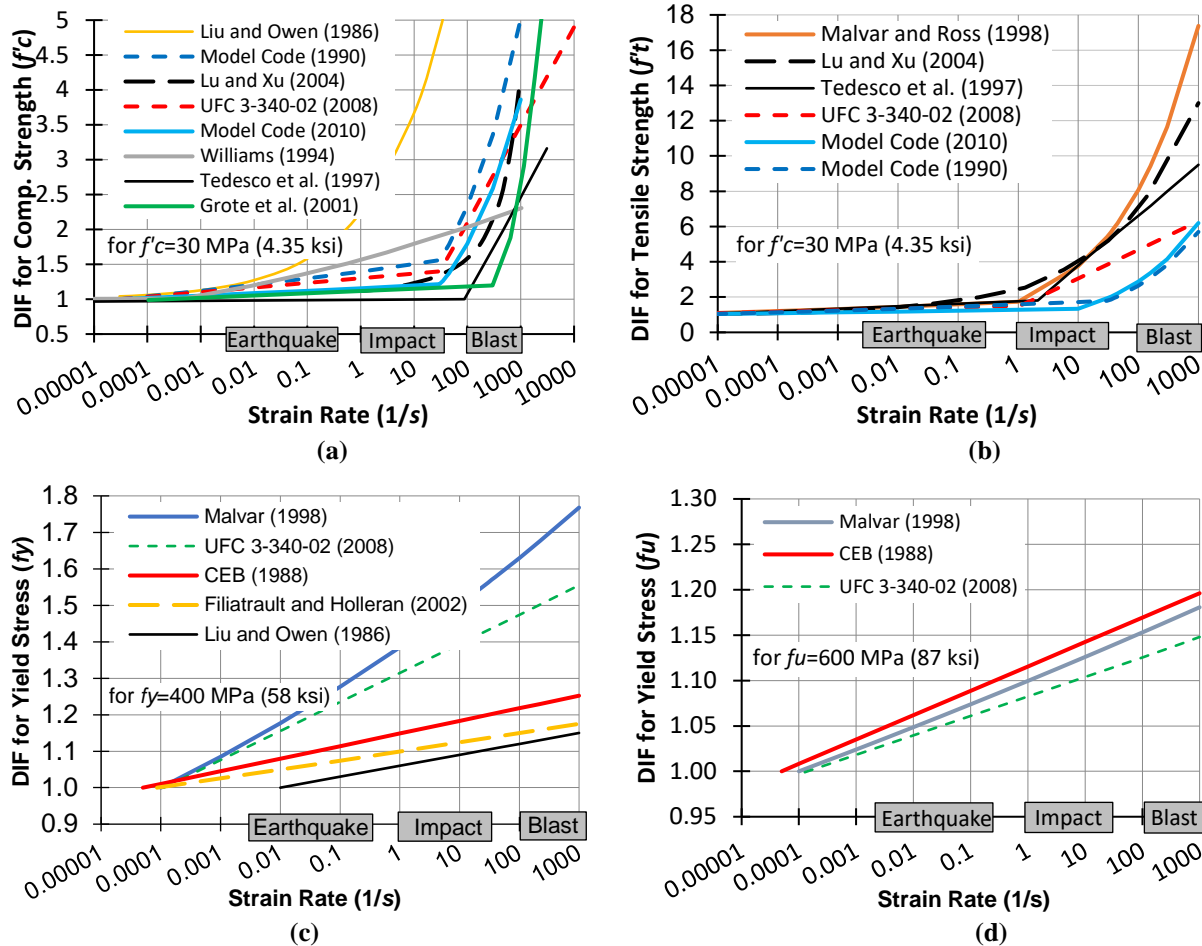


Fig. 3 – Strain rate - dynamic increase factor (DIF) relationships for: (a) concrete compressive strength; (b) concrete tensile strength; (c) reinforcing steel yield strength; (d) reinforcing steel ultimate strength (1 MPa = 0.145 ksi)

APPLICATION TO SIMPLIFIED FRAME ELEMENT MODELING

This section of the paper presents an overview of the frame modeling procedure and its application to eight previously tested beams subjected to twenty low-velocity (8.0 m/s or 26.2 ft/s) and high-mass (up to 600 kg or 1323 lb) impacts. The frame modeling procedure (Guner and Vecchio 2012, 2011, 2010) employs six-degree-of-freedom distributed-plasticity elements [see Fig. 4(a)] using an iterative, total-load, secant-stiffness formulation. A fiber discretization of the cross-section is employed, where the material stress and strain calculations are performed, as illustrated in Fig. 4(b). The layer elements are not discrete elements; rather, they represent the through-depth discretization of the section. There is, thus, no frictional assignments at layer interfaces. Each concrete and longitudinal reinforcing bar layer is defined as discrete elements while the transverse and out-of-plane reinforcement is smeared within the concrete layers. The out-of-plane reinforcement provides confinement to concrete layers. The main sectional compatibility requirement is that ‘plane sections remain plane,’ while the sectional equilibrium requirements include balancing the axial force, shear force, and bending moment (calculated by the global frame analysis). A parabolic shear strain distribution through the section depth is assumed, which reduces the computational demand greatly while allowing the simulation of the post-peak response at the same time. To compensate for the clamping stresses in the transverse direction (assumed to be zero), a shear protection algorithm is developed to prevent premature failures of D-regions. The mesh sensitivity studies are presented in Guner (2008). The fiber section approach provides advantages when modeling frames with unusual or complex cross-sections.

Model Creation, Analysis Execution, and Result Acquisition

Numerical models are created using the pre-processor program FormWorks Plus (Blosser et al. 2016, Sadeghian 2012), developed specifically for the VecTor suite of programs, which provides modeling capabilities in a Windows-based graphical environment with auto-meshing and sub-structuring facilities. The numerical analyses are conducted

using the computer program VecTor5 (VTAG 2019, Guner and Vecchio 2008). The analysis results are visualized using the post-processor program Janus (Loya et al. 2017, Chak 2013), which displays the displaced shape of the structure, crack widths, locations and propagation, rebar and concrete stresses and strains, and failure conditions. The post-processor program is a critical component of numerical modeling process since it aids analysts to understand the structural behavior, detect modeling mistakes, and effectively compare the calculated responses.

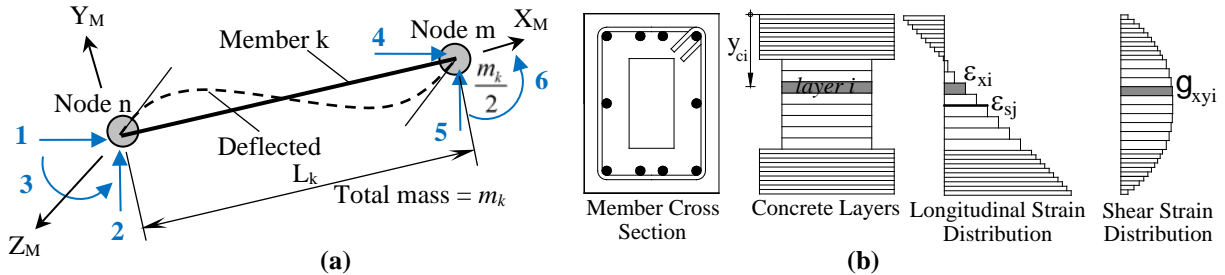


Fig. 4 – Frame-analysis procedure: (a) 6-dof frame element; (b) fiber section approach with strain distribution shown.

Application and Verification of Accuracy

The frame modeling procedure is verified, using only the default models and options, with eight previously tested specimens. The beam specimens, tested by Saatci and Vecchio (2009a) at the University of Toronto, include four pairs of beams subjected to free-falling weights, dropped from a clear height of 3.26 m (10.7 ft) above the specimens, resulting in an impact velocity of 8.0 m/s (26.2 ft/s). The beams were subjected to multiple testing, providing a total number of 20 impact tests. All beams had identical geometry, test setup, and longitudinal reinforcement details as shown in Fig. 5. The main variable was the amount of the transverse reinforcement, ranging from 0.0 to 0.3 %. The concrete strengths also varied slightly, ranging from 44.7 MPa to 50.1 MPa (6.5 to 7.3 ksi). The experimental program was comprised of Beams SS0 to SS3, where the numbers from 0 to 3 denote the transverse reinforcement ratios. The a-series and b-series beams were identical in all aspects except the loading protocol employed (see inset of Fig. 5).

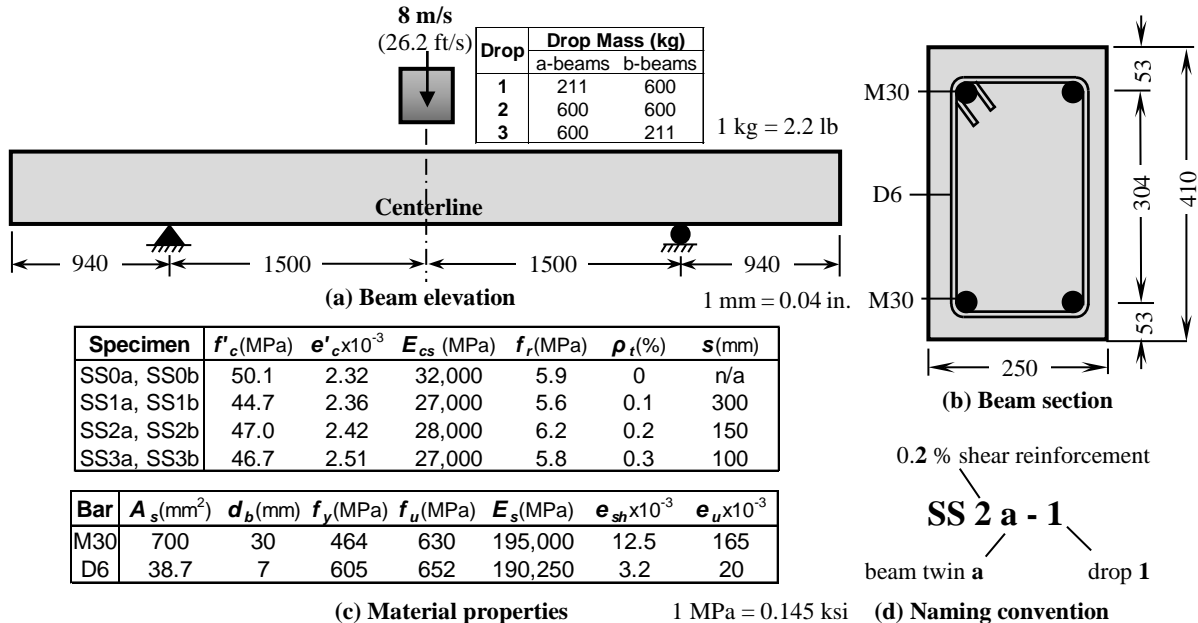


Fig. 5 – SS Beams Experimental Program Details for SS Beams (adopted from Saatci 2007)

The frame models are created for one-half of each beam as shown in Fig. 6. A special modeling technique, similar to that used by Saatci (2007), was employed to eliminate challenges associated with estimating the impact force history. For this, an impact transfer element (i.e., *Member 11*) was created. This element was assigned a very high stiffness to create a hard impact, and a linear-elastic compression-only behavior to permit the separation of the drop-weight from the beam after the impact. The impacting load was simulated by assigning an initial velocity of 8.0 m/s (26.2 ft/s) to

the mass defined at *Node 12*. The sectional models were created using 32 concrete layers in which the out-of-plane reinforcement ρ_z was smeared within a tributary area of 5 to 6 times the bar diameter d_b at each side of the horizontal legs of the stirrups. The longitudinal reinforcement was discretely modeled while the shear reinforcement was smeared into all layers except the clear cover layers, with the ratios shown in Fig. 6. Wilson's Theta Method, with no additional viscous damping and a time step length of 0.01 millisecond (ms), was used in all analyses.

The results are investigated in terms of the load-deflection responses, member deformations, concrete crack widths, reinforcement stresses and strains, the failure modes, and the failure displacements. The analysis results are visually verified through the graphical post-processor program Janus (Loya et al. 2015, Chak 2013). The peak displacements of the beams are calculated with excellent accuracy. Considering the 17 tests for which experimental peak displacement values are available (i.e., excluding broken sensor data), a mean value of 0.99 and a coefficient of variation (COV) of 9.5 % are achieved for the simulated-to-experimental ratios. Furthermore, the peak displacements of previously damaged specimens are captured remarkably well. For the second and third analyses of the damaged beams (10 tests), the mean ratio and COV of 0.98 and 7.1 % are obtained. The peak support reactions are also captured well. Considering all 20 simulations, a mean value of 0.95 and a COV of 21.3 % are obtained for the simulated-to-experimental ratios. These results are particularly remarkable considering the simplified modeling process (using line elements) and fast computational execution (10 minutes using a laptop computer with Intel Core i9-8950HK, 1 TB PCIe Class 50 SSD and 32 GB DDR4 memory). Selected response comparisons are presented in Fig. 7; refer to Guner (2008) for the complete set of comparisons. See also Saatci and Vecchio (2009b) for the analysis of these beams using a two-dimensional continuum finite element method.

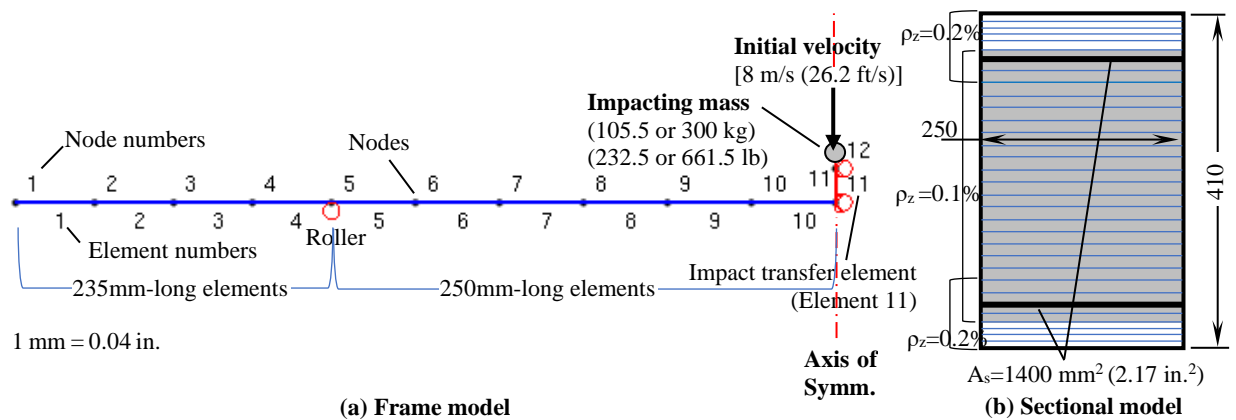


Fig. 6 – Frame model details for the SS Beams.

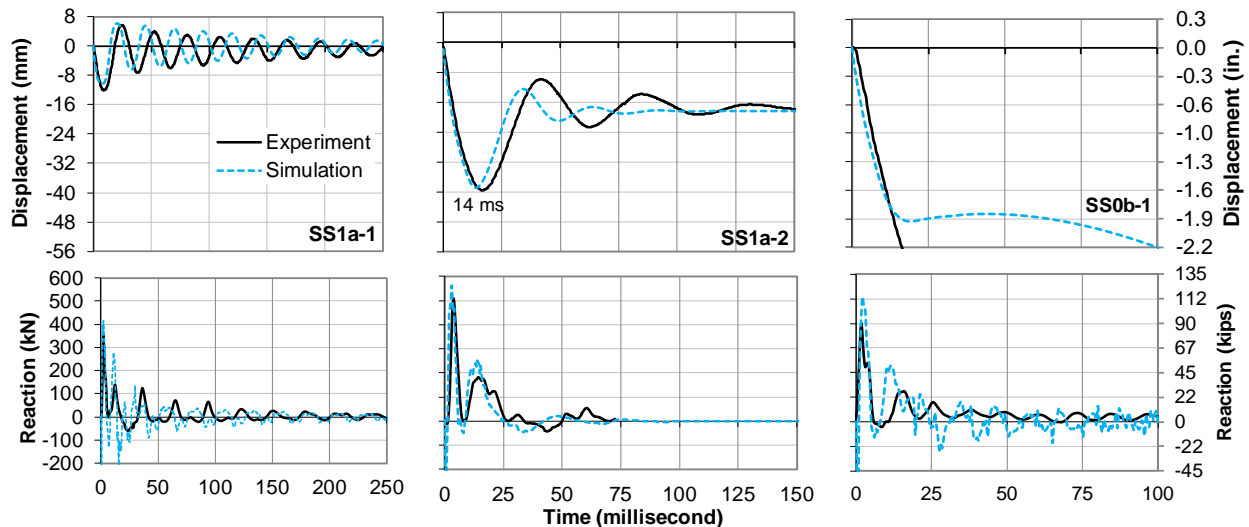


Fig. 7 – Midspan displacement and reaction responses for three sample beams

The post-peak damping characteristics, crack widths, damage levels (or failure modes when applicable) are predicted well. Although the procedure uses line elements, the stress, strain and cracking conditions are calculated and printed out for each layer of every element. The post-processor program Janus reads the output values and creates a two-dimensional rendering of the structure. Figure 8 shows sample renderings and compares them with the experimental results. The simulation procedure captured even the most severe cases of shear failures of Beams SS0a-2 and SS0b-1. It is worth pointing out that Beams SS2 and SS3 were designed as flexure-critical; when subjected to impact loads, however, they exhibited shear-dominated behaviors which is captured by the numerical procedure. This demonstrates the importance of employing a numerical modeling procedure (for impact loads) with shear-failure simulation capabilities even when modeling structures designed for flexural behavior under static loads.

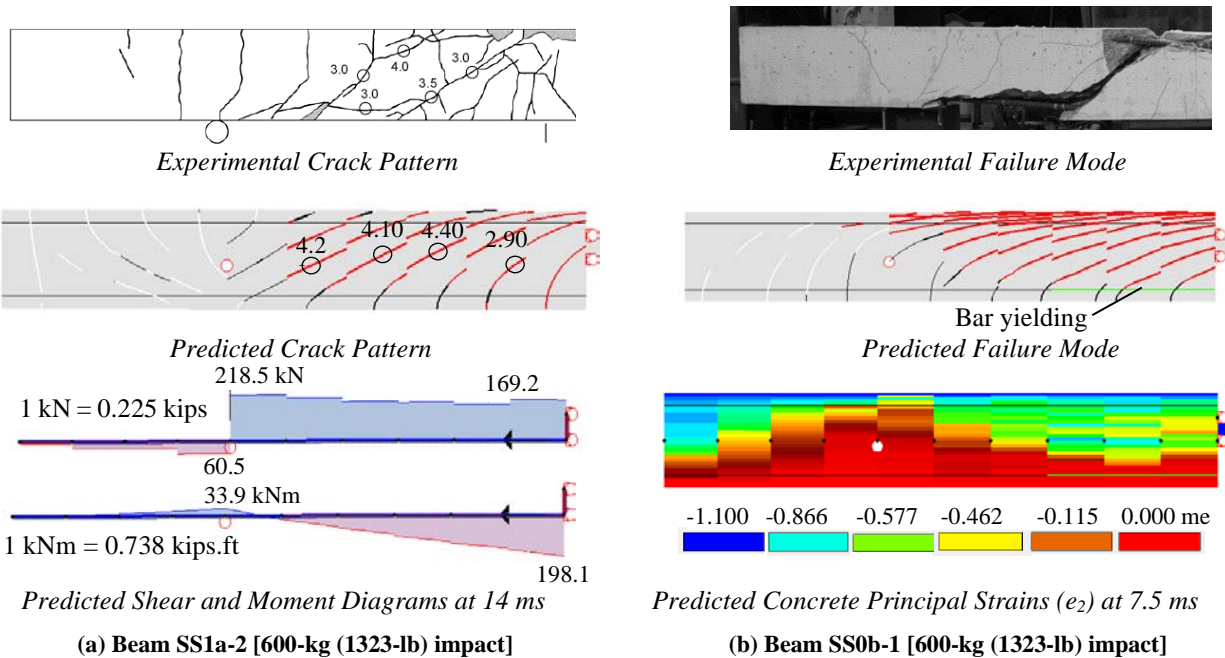


Fig. 8 – Sample simulation result for two beams (rendered by Janus)

Critical Modeling Aspects

The time step length has a significant impact on the accuracy of the results, stability of the calculation, and run time of the analysis. The analyses should be repeated for at least three different time step lengths to confirm that the simulation results do not change significantly with the use of smaller time steps. Both the displacement and support reaction responses should be investigated for this purpose – for example, Fig. 9(a) indicates that a time step length of 0.05 ms can be used; however, Fig 9(b) shows that a time step length of 0.01 ms provides a significantly different response and thus 0.01 ms should be used instead. A time step length of 0.005 ms, on the other end, provides a reaction response similar to 0.01 ms but doubles the analysis runtime. [see Fig. 9(c)]. A time step length in the order of the smallest natural vibration period of the structure (e.g., 0.03 ms for this beam) may be a good reference when determining the optimum time step length to use.

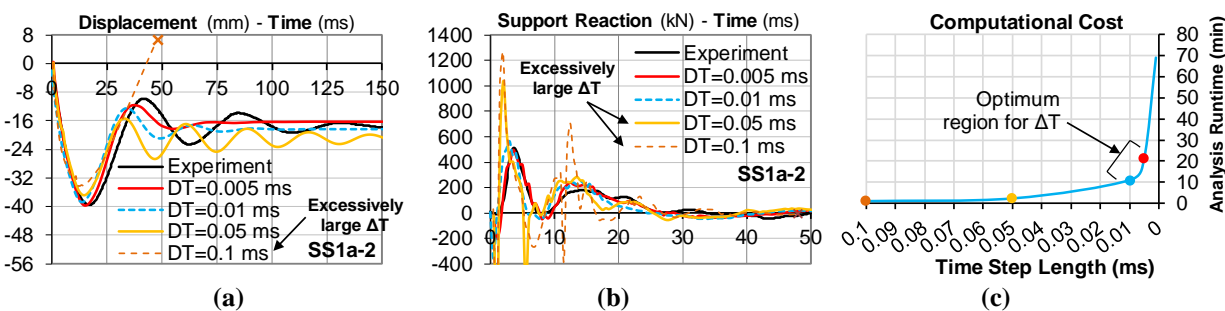


Fig. 9 – Determination of a valid time step length (ΔT) [1 mm =0.04 in.; 1 kN=0.225 kips]

The influence of the strain rate effects on the calculated responses are another important aspect of modeling. Fig. 10 shows the simulation results for two beams subjected to the same impact velocities (i.e., 8 m/s or 26.2 ft/s) but different impacting masses. In the case of a low-mass impact with no residual deformation, the strain rate formulations do not alter the results in any noticeable way [see Fig. 10(a)]. The strain rate effects become more important for impacts that create extensive damage and residual deformation [see Figs. 10(b) and (c)].

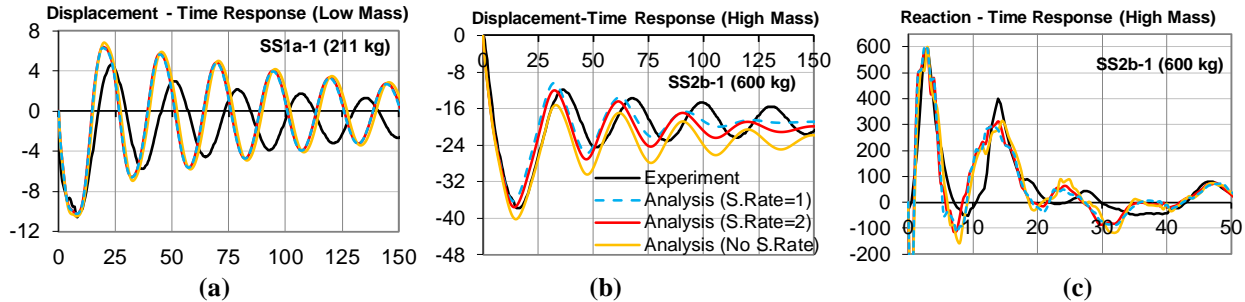


Fig. 10 – Influence of strain rate modeling [1 mm = 0.04 in.; 1 kN = 0.225 kips]

APPLICATION TO LAYERED THICK-SHELL FINITE ELEMENT MODELING

This section of the paper presents an overview of the layered thick-shell finite element modeling procedure and its application to the analysis of three RC slabs subjected to repeated high-mass, low-velocity impacts. The shell-based nonlinear finite element analysis procedure employs nine-node, 42-degree-of-freedom, layered ‘thick-shell’ finite elements and is principally dedicated to the analysis of RC planar structures such as slabs, walls, and curvilinear shell structures [refer to the example shown in Fig. 11(a)]. The layered formulation is used to account for variations of material stress, strain, and stiffness over the thickness of the shell elements. Layer stresses and strains are assumed constant over the height of each layer and the number of layers employed may be specified by the user [refer to Fig. 11(b)]. In-plane reinforcement can be defined in any planar orientation and is incorporated discretely within the depth of the element (i.e., in-plane reinforcement is not smeared or distributed throughout the concrete layers). Transverse reinforcement oriented in the out-of-plane direction is treated in a smeared sense and is considered in the material modeling of the core concrete layers. The through-thickness response of the layered thick-shell element is based on the assumptions that *i*) plane sections remain plane, but not necessarily normal to the element mid-surface, *ii*) out-of-plane normal stresses are negligible (Mindlin 1951) and, *iii*) according to the through-thickness formulation (presented in Hrynyk and Vecchio 2015), the ‘effective’ out-of-plane shear strain distribution used to calculate cracked concrete material response may be approximated as being parabolic through the thickness of the shell element. While these simplifying assumptions only approximately capture shell element deformation response, this approach negates the need for through-thickness finite element discretization and, in comparison to models generated using solid continuum meshing procedures, leads to significant reductions in the required number of degrees-of-freedom to create a model. The layered element concept and typical through-thickness sectional response conditions illustrating assumptions *i* and *iii* noted above are summarized in Fig. 11(b).

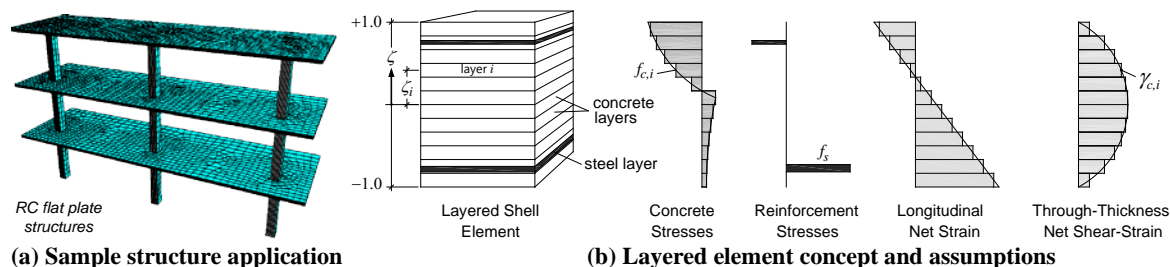


Fig. 11 – Layered thick-shell modeling applications and approach

Hrynyk-Vecchio Impact Slabs

For the purpose of illustrating the application of the shell element analysis procedure for impact response investigations, existing data from an experimental investigation performed at the University of Toronto (Hrynyk and

Vecchio 2014) is used. Seven intermediate-scale slabs, constructed with uniform geometries and loaded under repeated high-mass low-velocity impact, were tested. The slab-like elements were 1800-mm (71-in.) square, 130-mm (5.1-in.) thick, and were doubly reinforced in the orthogonal planar directions with mild steel reinforcement. Three of the seven slabs were constructed using a conventional concrete mixture design and four slabs were constructed using different steel fiber-reinforced concrete (SFRC) mixture designs. Note that for brevity, only the conventional RC slabs are presented in the subsequent modeling and analysis sections of this paper.

The cylindrical compressive strengths of the concretes comprising the conventional slabs ranged from 60 to 69 MPa (8.7 to 10 ksi) and the longitudinal reinforcement ratios of the slabs ranged from 0.27 to 0.59 % in each planar direction (per layer of steel). The typical reinforcement layout, the overall slab geometry, and the drop-weight test setup employed in the program are shown in Fig. 12. The slabs were restrained at their corners and impacted at their centers. Corner support assemblies restrained vertical translations but permitted spherical rotations and lateral slab expansions. The high-mass, low-velocity impact loads were generated using a drop-weight testing method. The striking face of the drop-weight consisted of a 25-mm (1.0-in.) thick, 300-mm (11.8-in.) square steel plate that produced a flat hard-impact loading condition. The weight was dropped from a constant height resulting in a nominal impact velocity of 8.0 m/s (26.2 ft/s). The loading protocol involved consecutive impacts of progressively increasing mass levels. The impact mass level for the conventional RC slabs ranged from 150 to 210 kg (331 to 463 lb) which corresponded to the application of either two or three consecutive impacts for each slab.

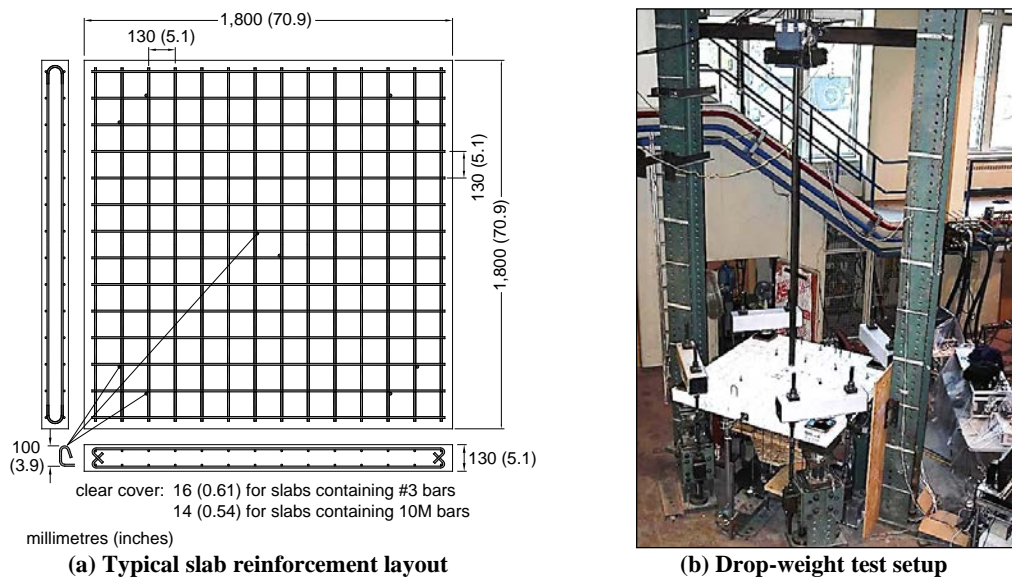


Fig. 12 – RC slab impact testing program (adapted from Hrynyk and Vecchio 2014)

Modeling Approach

In all cases, a common finite element mesh, consisting of a one-quarter slab thick-shell element model was used for the analyses of the impact-loaded slabs. In accordance with previously established guidelines developed on the basis of mesh sensitivity studies (Hrynyk 2013), sixty-five layered thick-shell elements and four out-of-plane truss bar elements were used to represent the quarter-slab specimens and the impacting drop-weight. Note that 64 of the shell elements comprised the RC slab and the drop-weight was modelled using a single shell element (refer to Fig. 13). A total of 298 nodes comprised the quarter-slab shell element mesh, resulting in a model with 1,295 total degrees-of-freedom. Note that, at least on the basis of the number of degrees-of-freedom, this represents relatively low-cost computational requirements when compared to the application of high-fidelity solid continuum modeling procedures that have been used to model the impact response of similar RC slab elements (e.g., Kishi et al. 2011). The shell elements forming the slab specimens were subdivided into 25 equal-thickness concrete layers, with an additional four layers provided to represent the four layers of in-plane longitudinal steel present in each of the slabs (see Fig. 13(c)).

To enforce symmetry, lateral and rotational restraints were provided along the slab centerlines forming the edges of the quarter-slab finite element model. The support reaction assemblies at the slab corners were incorporated by vertically restraining a single node within the quarter-slab mesh located at the center-point of the test frame reaction

assembly. The shell element simulating the drop-weight was connected to the shell elements forming the center-point impact region of the slab using four linear elastic ‘compression-only’ truss bar finite elements. The massless truss bar elements were assigned large stiffness values, simulating the hard impact loading scenario. Further, because the layered thick-shell finite elements employed rely on the assumptions that plane sections remain plane and out-of-plane normal stresses effects are negligible, local disturbances stemming from concentrated loads or, in this case, an impacting mass, are not inherently considered. In the context of shear resisting performance, neglecting out-of-plane confining or clamping stresses can lead to significant underestimation of the shear resistance of the shell elements comprising these regions (Goh and Hrynyk 2017). Thus, a form of out-of-plane shear strength enhancement, similar to the shear protection algorithm noted above in the description of the frame analysis procedure, was applied to the shell elements forming, and immediately surrounding, the impact regions of the slab (refer to Fig. 13). To enhance the shear strength of the disturbed elements, the net out-of-plane shear strains computed within these elements were reduced by a factor of two, resulting in an apparent shear stiffness enhancement. In assigning this shear strength enhancement, it was assumed that the disturbed region extended a distance equal to the effective reinforcement depth, d , away from the edges of the impacted area.

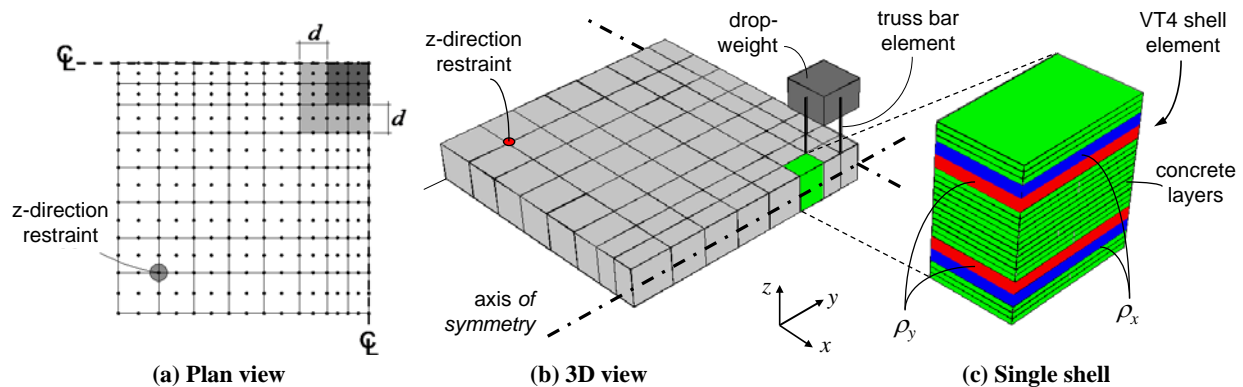


Fig. 13 - Quarter-slab thick-shell finite element model

Material modeling was conducted in accordance with the DSFM, using the material models summarized in Table 1, with two exceptions: *i*) Popovic’s High Strength Concrete model was used for the compression base curve to accommodate the higher-strength concretes used in the construction of the slabs, and *ii*) reinforcing bar buckling was neglected. Strain rate effects were incorporated using the default options summarized previously.

Impact loads were simulated by specifying an initial velocity of 8.0 m/s (26.2 ft/s) to four lumped masses assigned to the mid-side nodes of the rigid drop-weight shell element. Note that because the test slabs in the experimental program were subjected to sequential impact loading, it was necessary to perform a series of analyses for each slab specimen, with each analysis representing a single impact event. To facilitate the dynamic time stepping analysis within VecTor4, Newmark’s average acceleration method, with a constant time step of 0.1 ms, was considered for all impact events. Additionally, to aid in enhancing numerical stability, a constant level of supplemental stiffness proportional damping was considered. However, note that in all cases the level of proportional damping considered was quite small and resulted in damping ratios of less than 0.65 % of critical assigned to the first mode. Additional details regarding the evaluation of the minimum required supplement damping levels is presented elsewhere (Hrynyk and Vecchio 2017).

Results

The computed response-time histories for RC Slabs TH2, TH6, and TH7 are plotted alongside the experimental results in Figs. 14, 15, and 16, respectively. Note that the three RC slabs were nominally identical in terms of geometry and concrete; however, they were constructed with different longitudinal reinforcement ratios: 0.420 %, 0.273 %, and 0.592 % for slabs TH2, TH6, and TH7, respectively. In Fig. 14, the results from the first impact (TH2-1) and the third/final impact (TH2-3) are presented. In both cases, the shell-based analysis procedure is successful in capturing a number of occurrences in the observed impact responses. Specifically, the associated response periods and peak center-point displacement amplitudes are captured with high accuracy. Reasonable estimates are obtained for the response decay by way of the material hystereses, even with the use of only minimal levels of supplemental damping. In both impact events, peak reactions are significantly underestimated; however, it is worth noting that the computed

impulses associated with the reaction-time history responses are generally captured well. Finally, the analysis also successfully captured the punching failure mode that governed the responses of all three RC slabs. Figure 14(b) shows the computed displaced shape of Slab TH2 at the time of the peak center-point displacement and under the third and final impact. Fig. 15 presents results obtained for Slab TH6, which is the most lightly reinforced slab of the testing program and the only slab that exhibited punching under the second impact event (TH6-2). Similar levels of accuracy pertaining to the center-point displacement-time, reaction force-time, and impulse-time histories are obtained for Slab TH6 as are for Slab TH2.

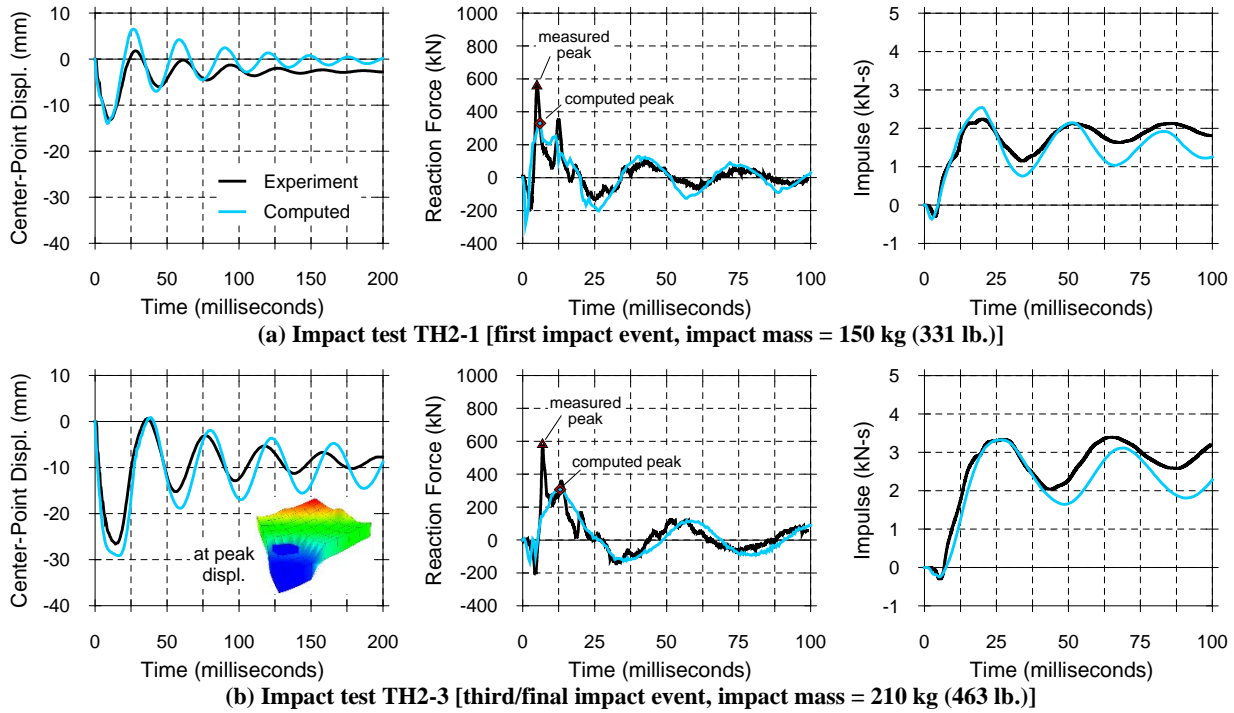
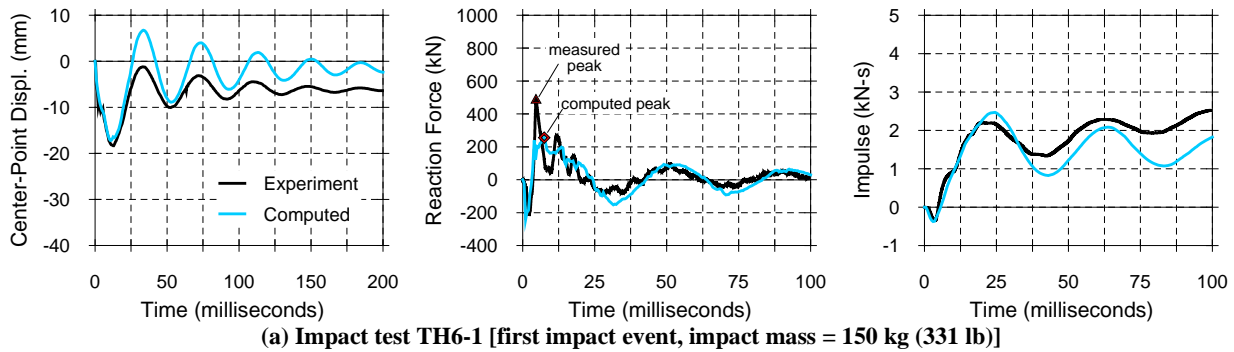


Fig. 14 - Computed response-time histories; RC Slab TH2 ($\rho_1 = 0.420\%$) [1 mm = 0.04 in.; 1 kN = 0.225 kip]



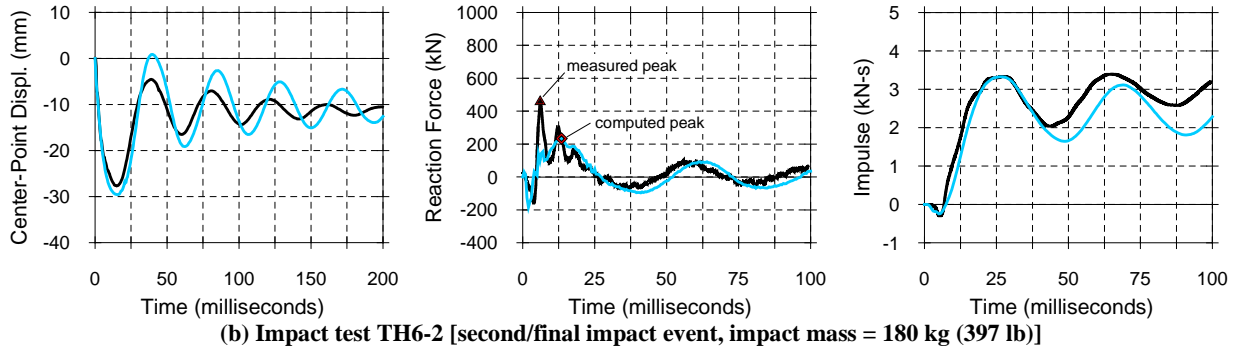


Fig. 15 - Computed response-time histories; RC Slab TH6 ($\rho_1 = 0.273\%$) [1 mm = 0.04 in.; 1 kN = 0.225 kip]

In Fig. 16, the observed and computed displacement-time histories for Slab TH7 are presented. While high-quality estimates are obtained for the peak center-point displacement amplitudes in the first two impact events, the shell-based analysis procedure underestimated the severity of the slab punching that occurred in the third and final impact event (TH7-3). As a result, the computed response slightly underestimated the peak displacement amplitude, and significantly underestimated the residual displacement.

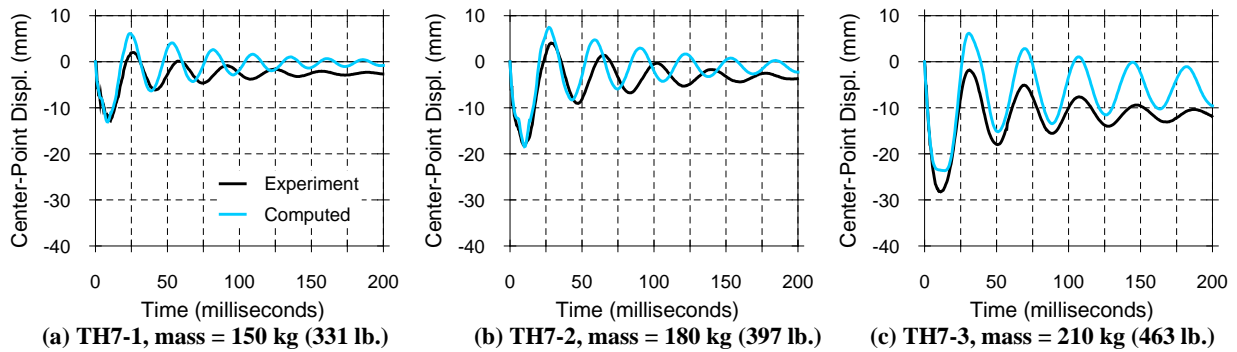


Fig. 16 - Computed displacement-time histories; RC Slab TH7 ($\rho_1 = 0.592\%$) [1 mm = 0.04 in.; 1 kN = 0.225 kip]

The general trends noted above regarding the computed responses are apparent from the summary provided in Fig. 17. Again, in nearly all cases, the center-point peak displacement amplitudes and the peak impulse values associated with the slab reaction are computed consistently and with good accuracy for the eight impact events performed on the RC slabs. However, as noted previously, the computed peak reaction forces are significantly underestimated in all cases. It is likely that the underestimation of the peak reaction is a byproduct of the simplified modeling approach employed, particularly with respect to the modeling of the support conditions. Recall, no attempt was made to model the physical test frame or support structure employed in the experiments.

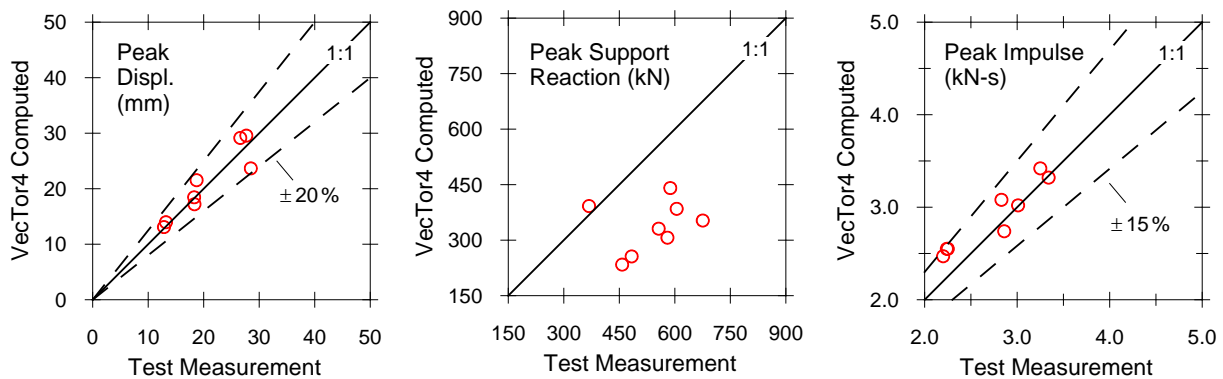


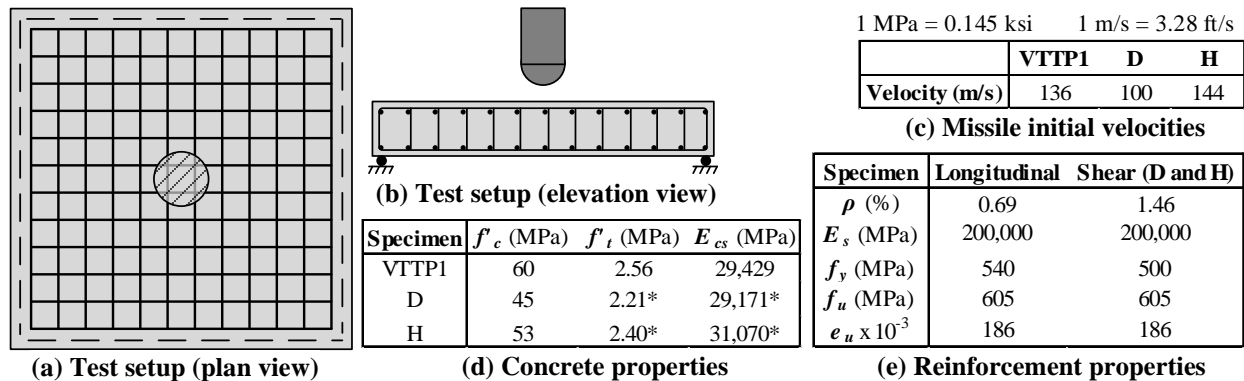
Fig. 17 - Summary of results for Hrynyk-Vecchio RC impact slabs [1 mm = 0.04 in.; 1 kN = 0.225 kip]

APPLICATION TO SOLID CONTINUUM AND AXISYMMETRIC FINITE ELEMENT MODELING

The following section of the paper presents an overview and application of two structural analysis procedures: 1) 3D solid rectangular (employing 24-degrees-of-freedom), 2) 2D axisymmetric (employing 8-degrees-of-freedom) finite elements, where the target and the impactor are generated by the rotation of the 2D axisymmetric plane finite elements around the axis of symmetry. Previously tested RC wall specimens are modeled subject to hard missile impacts, with two impactors that completely perforated the specimens and exited with residual velocities, and one impactor that was stopped by the target. Significant local deformations due to slab perforation is modeled using element erosion and reinforcement rupture formulations. The simulation results are compared with the experimental data and are evaluated in terms of the residual velocities of the missiles and the deformed shapes of the targets.

Test Specimens

Three hard missile impact tests were modeled using the two procedures. One of the test specimens, VTTP1, was the subject of a blind competition in the *Improving Robustness Assessment Methodologies for Structures Impacted by Missiles* (IRIS 2010) workshop (NEA 2014). All three specimens were tested by VTT Technical Research Center of Finland. The specimens consisted of 2100 x 2100 x 250 mm (83 x 83 x 10 in.) RC panels with two layers of 10-mm (3/8 in.) diameter longitudinal bars at a spacing of 90 mm (3.5 in.) in both directions. 12 mm (0.5 in.) T-bars on a 90 x 90 mm (3.5 x 3.5 in.) grid were provided as shear reinforcement for Specimens D and H, whereas no shear reinforcement was used in VTTP1. The test setup, concrete and steel material properties are presented in Fig. 18.



* estimated values (not reported in the experiments)

Fig. 18 – Missile impact test setup and material properties (adopted from NEA 2014, Vepsä et al. 2012, Orbovic and Blahoianu 2011, Orbovic et al. 2009)

Model Creation

The analysis model using 3D solid elements is shown in Fig. 19(a). Quarter-panel models are used to reduce computational time; the faces on the axes of symmetry were restrained with roller supports in the appropriate directions. A total of 5,760 rectangular 8-node hexahedral elements are used to model the concrete component of each panel. The shear reinforcement was modeled as smeared reinforcement for Specimens D and H while the longitudinal reinforcement was modeled using 1,104 discrete truss bar elements that are shown through the cut on the left side of the panel in Fig. 19(a). The missile was connected to the target by way of nine compression-only truss bars.

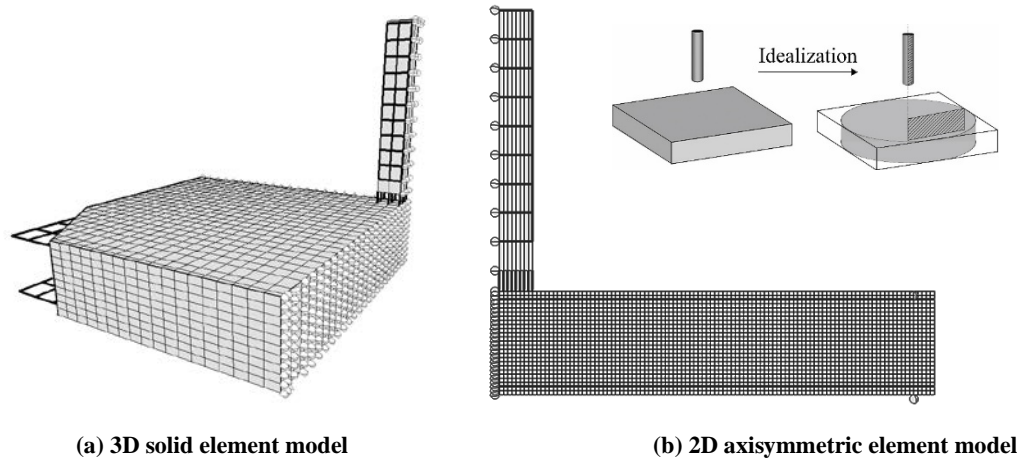


Fig. 19 – Quarter-wall and axisymmetric finite element models.

The analysis model using axisymmetric elements is shown in Fig. 19(b). The figure illustrates the idealization of a square panel as a circular panel with a diameter equal to the length of the specimen. A total of 2,697 4-node rectangular torus elements with a size of 10 mm x 10 mm (0.4 x 0.4 in.) were used to model the concrete component of each panel. Additionally, 210 truss elements were used to model the longitudinal reinforcement. The area of the truss elements was adjusted to keep the reinforcement ratio constant through the panel. The shear reinforcement was modeled as smeared reinforcement through the concrete elements for Specimens D and H. The concrete fill and steel head of the missiles were modeled using 72 4-node rectangular torus elements while the steel tube is modeled using 80 truss elements. The missile and the panels were connected with nine compression-only truss elements. For both modeling approaches, mesh density is determined in accordance with the mesh sensitivity analyses presented by Lulec (2017). Since, an axisymmetric element has less degrees-of-freedom than a solid element, modeling with axisymmetric elements requires less computational power than modeling with 3D solid elements. However, both the geometry of the structure and the loading should be axisymmetric to use this modeling procedure.

Material Modeling and Analysis Parameters

Material modeling was conducted in accordance with the DSFM, using the material models summarized in Table 1, with two exceptions: *i*) Hoshikuma et al. (1997) high Strength Concrete model was used for the compression base curve to accommodate the higher-strength concretes used in the construction of the specimens, and *ii*) strain rate effects were only considered for the steel reinforcement. Additionally, to model the local deformation due to penetration of the missiles, element erosion criteria based on shear and principal tensile strains were utilized in accordance with the previously determined guidelines (Lulec 2017).

Results

The missile residual velocities obtained from the simulations and the experiments are summarized in Fig. 20. For Specimen D, the missile rebounded leaving an impact depth of 38 mm, while the missiles perforated through with residual velocities for Specimens H and VTTP1. Both modeling approaches capture the perforation/rebounding of the missiles. The residual velocities obtained from the simulations are in good agreement with the experimental results. Moreover, the impact depths calculated from the simulations with solid elements and axisymmetric elements are 33 mm (1.25 in.) and 32 mm (1.25 in.), respectively.

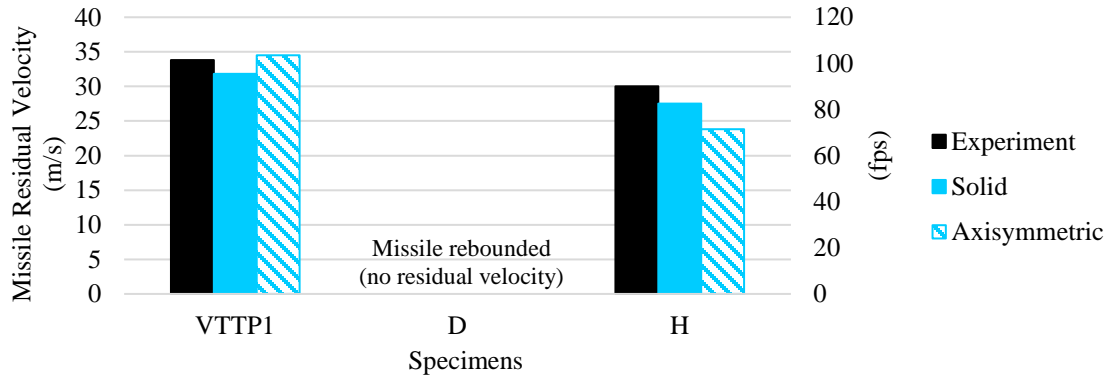


Fig. 20 – Missile residual velocities

The deformed shapes and perforation/rebounding response of the missiles, as obtained from the numerical simulations, are shown in Fig. 21. Additionally, the damage surfaces created on the front and back faces of the targets due to the perforation of the missile for the specimens are shown in Fig. 22 for Specimens VTTP1 and H. The simulation results match well with the experimental observations. In the front faces, simulations using solid elements resulted in bigger holes than those using the axisymmetric elements. One possible reason for this is the difference in the mesh sizes used in each modeling approach. Capturing local deformations on the front face becomes harder with the increasing coarseness of the mesh since the hole diameter on the front face is relatively small compared to the mesh size used for solid elements.

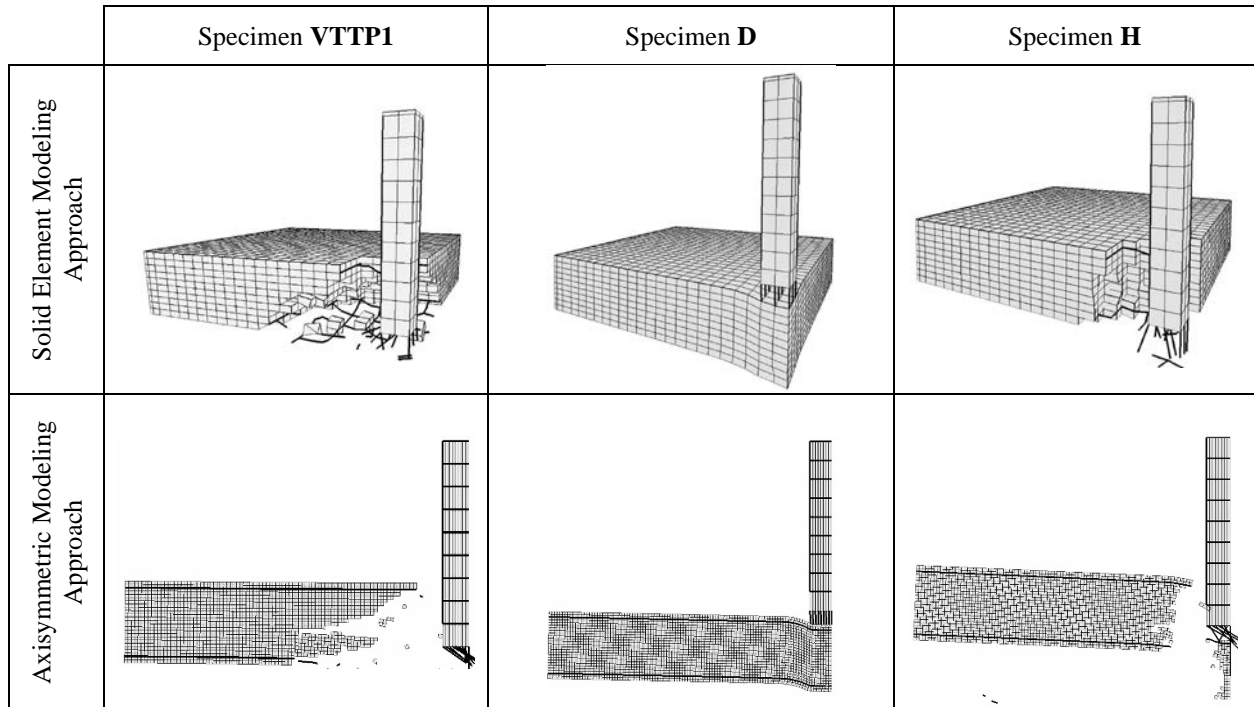


Fig. 21 – Deformed shapes of wall specimens estimated by way of solid and axisymmetric finite element models

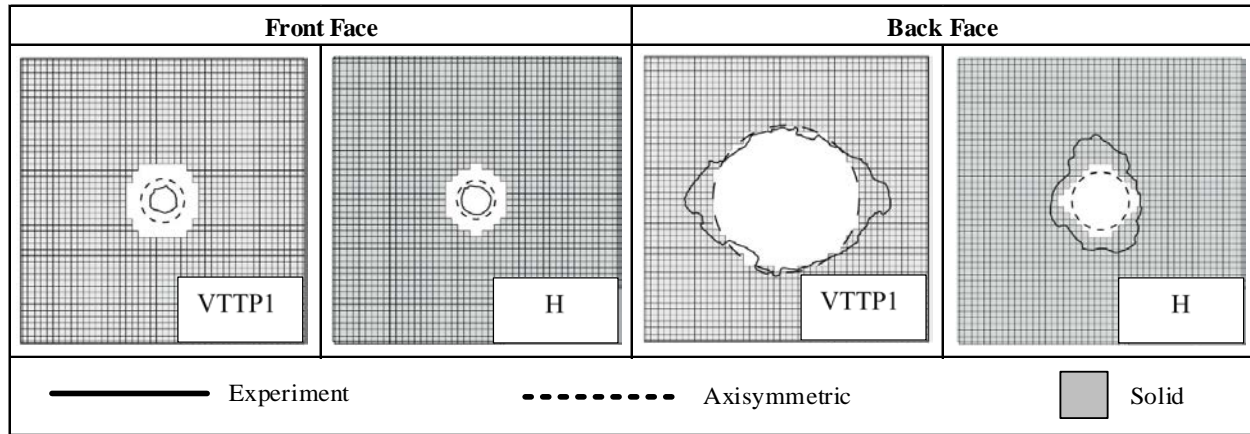


Fig. 22 – Damaged surfaces for RC wall specimens VTTP1 and H

SUMMARY AND CONCLUSIONS

In this study, a comprehensive modeling methodology incorporating four different structural analysis procedures (using 2D frames, 3D thick-shells, 3D solids, and 2D axisymmetric finite elements) are presented for impact load analysis of RC structures. The material modeling methodology, which is common amongst all four modeling procedures, employs a smeared-crack continuum approach based on the constitutive formulations of the DSFM. Key results obtained from the studies presented in this paper support the following main conclusions:

1. Impact-load modeling of concrete elements requires comprehensive and fast analysis tools. Pre- and post-processor software is essential in understanding the behavior and the failure mode of the structures by showing the sequence of nonlinear events, crack propagation, concrete and reinforcement stresses/strains, perforation/rebounding response and residual velocity of the impacting mass, and the deflected shapes.
2. The Disturbed Stress Field Model can successfully be employed within an explicit time-step integration method for simulating the RC material behavior subjected to impact loads while inherently accounting for the influence of transverse shear within the nonlinear dynamic analyses.
3. The total-load and secant-stiffness-based solution algorithm exhibits excellent convergence and numerical stability characteristics even in the heavily damaged and post-impact stages of the responses.
4. Impact analyses can simply and accurately be performed using a fictitious transfer element incorporating the impacting mass and the contact velocity. This eliminates the uncertainties associated with estimating the impact force history as the analysis input.
5. The time step length has a significant impact on the accuracy of the results, stability of the solution, and run time of the analysis. The analyses should be repeated for at least three different time step lengths to confirm that both the displacement and reaction results do not change significantly. In this study, a time-step length in the order of the smallest vibration period provided a suitable balance between the computational accuracy and cost.
6. The nonlinear modeling methodology presented in this study employs simple structural models, incorporates experimentally verified default material models (without requiring calibration studies), and requires short analysis times.
7. The methodology incorporating four different structural analysis procedures accurately simulate the experimental behaviors of the specimens including peak deflections, strengths, stiffnesses, residual deflections, and damage and failure modes (including shear failures), and missile residual velocities and perforation/rebounding behavior.

ACKNOWLEDGMENT

The authors would like to thank Dr. Frank J. Vecchio for the technical guidance he provided over the course of the studies of all three authors, and Dr. Selcuk Saatci for the experimental data of the SS beams examined in this study. The authors acknowledge the support of the Natural Sciences and Engineering Research Council of Canada (NSERC).

REFERENCES

- Akkaya, Y., Guner, S., and Vecchio, F. J. (2019) "Constitutive Model for the Inelastic Buckling Behavior of Reinforcing Bars," *ACI Structural Journal*, Vol. 116, No. 3, pp. 195-204. Retrieved from https://www.utoledo.edu/engineering/faculty/serhan-guner/docs/JP11_Akkaya_et_al_2019.pdf
- Asprone, D., Cadoni, E., and Prota, A. (2009) "Tensile High Strain-Rate Behavior of Reinforcing Steel from an Existing Bridge," *ACI Structural Journal*, Vol. 106, No. 4, pp. 523-529.
- Blosser K, Guner S, and Vecchio F. J. (2016) "User's Manual of FormWorks Plus for VecTor5," Online Publication, 29 pp. Retrieved from http://www.utoledo.edu/engineering/faculty/serhan-guner/docs/M3_VT5FWPManual.pdf
- CEB (1988) "Concrete Structures under Impact and Impulsive Loading - Synthesis Report," Comité EURO-International du Béton, Bulletin D'Information, No. 184, 184 pp.
- CEB-FIP (1990) "Model Code for Concrete Structures," Design Code, Comité EURO International du Béton, 437 pp. Retrieved from <https://www.fib-international.org/publications/ceb-bulletins/ceb-fip-model-code-90-pdf-detail.html>
- Chak I.N. (2013) "Janus: A Post-Processor for VecTor Analysis Software," MAsc Thesis, Department of Civil Engineering, University of Toronto, ON, Canada, 193 pp. Retrieved from [http://www.vectoranalysisgroup.com/theses/Chak-MASc\(2013\).pdf](http://www.vectoranalysisgroup.com/theses/Chak-MASc(2013).pdf)
- El-Dakhkhni, W. W., Mekky, W. F., and Changiz Rezaei, S. H. (2010) "Validity of SDOF Models for Analyzing Two-Way Reinforced Concrete Panels under Blast Loading," *Journal of Performance of Constructed Facilities*, ASCE, Vol. 24, No. 2, pp. 311-325.
- fib* Model Code (2010) "*fib* Model Code for Concrete Structures," Ernst & Sohn, Oct. 2013, 434 pp. Retrieved from <https://onlinelibrary.wiley.com/doi/book/10.1002/9783433604090>
- Filiatrault, A. and Holleran, M. (2002) "Stress-Strain Behavior of Reinforcing Steel and Concrete under Seismic Strain Rates and Low Temperatures," *Materials and Structures*, Vol. 34, No. 4, pp. 235-239.
- Grote, D. L., Park, S. W., and Zhou, M. (2001) "Dynamic Behavior of Concrete at High Strain Rates and Pressures: I. Experimental Characterization," *International Journal of Impact Engineering*, Vol. 25, No. 9, pp. 869-886.
- Goh, C. and Hrynyk, T.D. (2017) "Toward Practical Modelling of Reinforced Concrete Flat Slab Systems," Proceedings of the 39th IABSE Symposium: Engineering the Future, Vancouver, Canada, ISBN: 978-3-85748-153-6.
- Guner, S. (2008) "Performance Assessment of Shear-Critical Reinforced Concrete Plane Frames," PhD Dissertation, Department of Civil Engineering, University of Toronto, 429 pp. Retrieved from https://www.utoledo.edu/engineering/faculty/serhan-guner/docs/T2_Guner_PhD_2018.pdf
- Guner, S. and Vecchio F. J. (2008) "User's Manual of VecTor5," Online publication, 88 pp. Retrieved from <http://www.utoledo.edu/engineering/faculty/serhan-guner/docs/M1-VT5Manual-V1.2.pdf>
- Guner, S. and Vecchio, F. J. (2010) "Pushover Analysis of Shear-Critical Frames: Formulation," *ACI Structural Journal*, Vol. 107, No. 1, pp. 63-71. Retrieved from http://www.utoledo.edu/engineering/faculty/serhan-guner/docs/JP1_Guner_Vecchio_2010a.pdf
- Guner, S. and Vecchio, F. J. (2011) "Analysis of Shear-Critical Reinforced Concrete Plane Frame Elements under Cyclic Loading," *Journal of Structural Engineering*, ASCE, Vol. 137, No. 8, pp. 834-843. Retrieved from <https://ascelibrary.org/doi/abs/10.1061/%28ASCE%29ST.1943-541X.0000346>
- Guner, S. and Vecchio, F. J. (2012) "Simplified Method for Nonlinear Dynamic Analysis of Shear-Critical Frames," *ACI Structural Journal*, Vol. 109, No. 5, pp. 727-737. Retrieved from www.utoledo.edu/engineering/faculty/serhan-guner/docs/JP4_Guner_Vecchio_2012.pdf

Hoshikuma, J., Kawashima, K., Nagaya, K., Taylor, A.W. (1997) "Stress-Strain Model for Confined Reinforced Concrete in Bridge Piers," *Journal of Structural Engineering*, ASCE, Vol.123, No.5, pp. 624-633.

Hrynyk, T.D. (2013) "Behaviour and Modelling of Reinforced Concrete Slabs and Shells Under Static and Dynamic Loads," PhD Dissertation, Dept. of Civil Engineering, University of Toronto, ON, Canada, 455 pp.

Hrynyk, T.D. and Vecchio, F.J. (2014) "Behavior of Steel Fiber-Reinforced Concrete Slabs under Impact Load," *ACI Structural Journal*, 111(5), pp. 1213-1224.

Hrynyk, T.D. and Vecchio, F.J. (2015) "Capturing Out-of-Plane Shear Failures in the Analysis of Reinforced Concrete Shells," *Journal of Structural Engineering*, ASCE, DOI: 10.1061/(ASCE)ST.1943-541X.0001311.

Hrynyk, T.D. and Vecchio, F.J. (2017) "Modeling of Reinforced and Fiber-Reinforced Concrete Slabs under Impact Loads," *ACI SP-321 'Recent Developments in Two-Way Slabs: Design, Analysis, Construction and Evaluation'*, pp. 8.1-8.20, ISBN-13: 978-1-945487-76-7.

Kent, D. C., and Park, R. (1971) "Flexural Members with Confined Concrete," *ASCE Journal of the Structural Division*, Vol. 97, No. ST7, Proc. Paper 8243, pp. 1341-1360.

Kishi, N., Kurihashi, Y., Ghadimi Khasraghy, S., and Mikami, H. (2011) "Numerical Simulation of Impact Response Behavior of Rectangular Reinforced Concrete Slabs Under Falling-Weight Impact Loading," *Applied Mechanics and Materials*, V. 82, pp. 266-271.

Kupfer, H., Hilsdorf, H.K., and Rusch, H. (1969) "Behavior of Concrete under Biaxial Stress," *ACI Journal*, Vol. 87, No. 2, pp. 656-666.

Liu, G. Q. and Owen, D. R. J. (1986) "Ultimate Load Behaviour of Reinforced Concrete Plates and Shells under Dynamic Transient Loading," *International Journal for Numerical Methods in Engineering*, Vol. 22, No. 1, pp. 189-208.

Loya A. S., Lourenço D. D. S., Guner S., Vecchio F. J. (2017) "User's Manual of Janus for VecTor5," Online Publication, 28 pp. Retrieved from http://www.utoledo.edu/engineering/faculty/serhan-guner/docs/M2_VT5JanusManual_V2.0.pdf

Lu, Y. and Xu, K. (2004) "Modelling of Dynamic Behaviour of Concrete Materials under Blast Loading," *International Journal of Solids and Structures*, Vol. 41, No. 1, pp. 131-143.

Lulec, A. (2017) "Simplified Analytical Tools for Impact and Impulsive Loading Analysis of Reinforced Concrete Structures," PhD Dissertation, Dept. of Civil Engineering, University of Toronto, ON, Canada, 139-146 pp.

Malvar, L. J. (1988) "Review of Static and Dynamic Properties of Steel Reinforcing Bars," *ACI Materials Journal*, Vol. 95, No. 5, pp. 609-614.

Malvar, L. J. and Ross, C. A. (1998) "Review of Strain-Rate Effects for Concrete," *ACI Materials Journal*, Vol. 95, No. 6, pp. 735-739.

Mander, J. B., Priestley, M. J. N., and Park. R. (1988) "Theoretical Stress-Strain Model for Confined Concrete," *ASCE Journal of Structural Engineering*, Vol. 114, No. 8, pp. 1804-1826.

Mindlin, R.D. (1951) "Influence of Rotary Inertia and Shear on Flexural Motions of Isotropic, Elastic Plates," *ASME Journal of Applied Mechanics*, 18(1), pp. 31-38.

Newmark, N. M. (1959) "A Method of Computation for Structural Dynamics," *Journal of the Engineering Mechanics Division ASCE*, Vol. 85, No. 3, pp. 67-94.

Nuclear Energy Agency (2014) "Improving Robustness Assessment Methodologies for Structures Impacted by Missiles," (IRIS_2012): Final Report. Retrieved from <https://www.oecd-nea.org/nsd/docs/2014/csni-r2014-5.pdf>

Orbovic, N., Elgoharyb, M., Leeb, N., Blahoianu, A. (2009) "Tests on Reinforced Concrete Slabs with Pre-Stressing and with Transverse Reinforcement under Impact Loading," *Transactions of International Conference – SMiRT 20*, Espo, Finland.

Orbovic, N. and Blahoianu, A. (2011) "Tests on Concrete Slabs under Hard Missile Impact to Evaluate the Influence of Transverse Reinforcement and Pre-Stressing on Perforation," *Transactions of International Conference – SMiRT 21*, New Delhi, India.

Popovics, S. (1973) "A Numerical Approach to the Complete Stress-Strain Curve of Concrete," *Cement and Concrete Research*, Vol. 3, No. 5, pp. 583-599.

Richart, F. E., Brandtzaeg, A., and Brown, R.L. (1928) "A Study of the Failure of Concrete under Combined Compressive Stresses," Bulletin No. 185, University of Illinois Engineering Experimental Station, Urbana, Illinois, 104 pp.

Saatci, S. (2007) "Behaviour and Modelling of Reinforced Concrete Structures Subjected to Impact Loading," PhD Thesis, Department of Civil Engineering, University of Toronto, ON, Canada, 288 pp. Retrieved from http://www.vectoranalysisgroup.com/theses/thesis_saatci.pdf

Saatci, S., and Vecchio, F. J. (2009a) "Effects of Shear Mechanisms on Impact Behavior of Reinforced Concrete Beams," *ACI Structural Journal*, Vol. 106, No. 1, pp. 78-86. Retrieved from http://www.vectoranalysisgroup.com/journal_publications/jp65.pdf

Saatci, S., and Vecchio, F. J. (2009b) "Nonlinear Finite Element Modeling of Reinforced Concrete Structures under Impact Loads," *ACI Structural Journal*, Vol. 106, No. 5, pp. 717-725. Retrieved from http://www.vectoranalysisgroup.com/journal_publications/jp67.pdf

Sadeghian V. (2012) "Formworks-Plus: Improved Pre-Processor for Vector Analysis Software," MASC Thesis, Department of Civil Engineering, University of Toronto, Canada, ON, Canada 147 pp. Retrieved from [http://www.vectoranalysisgroup.com/theses/Sadeghian-MASc\(2012\).pdf](http://www.vectoranalysisgroup.com/theses/Sadeghian-MASc(2012).pdf)

Scott, B. D., Park, R., and Priestley, M.J.N. (1982) "Stress-Strain Behavior of Concrete Confined by Overlapping Hoops at Low and High Strain Rates," *ACI Journal*, Vol. 79, No. 1, pp.13-27.

Seckin, M. (1981) "Hysteretic Behaviour of Cast-in-Place Exterior Beam-Column-Slab Subassemblies," PhD Dissertation, Department of Civil Engineering, University of Toronto, ON, Canada, 236 pp.

Tedesco, J. W., Powell, J. C., Allen Ross, C., and Hughes, M. L. (1997) "A Strain-Rate-Dependent Concrete Material Model for Adina," *Computers and Structures*, Vol. 64, No. 5-6, pp. 1053-1067.

UFC 3-340-02 (2008) "Structures to Resist the Effects of Accidental Explosions," Unified Facilities Criteria, U.S. Army Corps of Engineers, 1943 pp. Retrieved from https://www.wbdg.org/FFC/DOD/UFC/ufc_3_340_02_2008_c2.pdf

Vecchio F. J. (1999) "Towards Cyclic Load Modeling of Reinforced Concrete," *ACI Structural Journal*, Vol. 96, No. 2, pp. 193-202. Retrieved from http://www.vectoranalysisgroup.com/journal_publications/jp29.pdf

Vecchio, F. J. (2000) "Disturbed Stress Field Model for Reinforced Concrete: Formulation," *Journal of Structural Engineering*, ASCE, Vol. 126, No. 9, pp. 1070-1077. Retrieved from http://www.vectoranalysisgroup.com/journal_publications/jp34.pdf

Vecchio, F. J. and Collins, M. P. (1986) "The Modified Compression-Field Theory for Reinforced Concrete Elements subjected to Shear," *ACI Journal*, Vol. 83, No. 2, pp. 219-231. Retrieved from http://www.vectoranalysisgroup.com/journal_publications/jp2.pdf

VecTor5 (2019) "A Nonlinear Finite Element Analysis Program for Two-Dimensional Reinforced Concrete Frame Structures," Computer software, VecTor Analysis Group (VTAG). Retrieved from <http://www.vectoranalysisgroup.com>

Vepsä, A., Saarenheimo, A., Tarallo, F., Rambach, J. M., and Orbovic, N. (2012) "Impact Tests for IRIS 2010 Benchmark Exercise," *Journal of Disaster Research*, Vol. 7, No. 5, pp. 619-628.

Williams, M. S. (1994) "Modeling of Local Impact Effects on Plain and Reinforced Concrete," *ACI Structural Journal*, Vol. 91, No. 2, pp. 178-187.

Wilson, E. L., Farhoomand, I., and Bathe K. J. (1973) "Nonlinear Dynamic Analysis of Complex Structures," *Earthquake Engineering and Structural Dynamics*, Vol. 1, No. 3, pp.241-252.

Wong, P. S., Vecchio, F. J., and Trommels, H. (2013) "VecTor2 and FormWorks User's Manual," Technical Report, VecTor Analysis Group (VTAG), 347 pp. Retrieved from http://www.vectoranalysisgroup.com/user_manuals/manual1.pdf.